

Article

Biophysical Effects of Land Cover Changes on Land Surface Temperature on the Sichuan Basin and Surrounding Regions

Xiangming Mao ^{1,*}, Gula Tang ², Jiaqiang Du ^{3,4} and Xiaotong Tian ²¹ Law School, Panzhihua University, Panzhihua 617000, China² Guokechuang (Beijing) Information Technology Co., Ltd., Beijing 100070, China; tang@guokc.com (G.T.)³ State Key Laboratory of Environmental Criteria and Risk Assessment, Chinese Research Academy of Environmental Sciences, Beijing 100012, China; dujq@craes.org.cn⁴ State Environmental Protection Key Laboratory of Regional Eco-Process and Function Assessment, Chinese Research Academy of Environmental Science, Beijing 100012, China

* Correspondence: maoxiangming@pzhu.edu.cn

Abstract: The biophysical effect of land cover changes (LCC) on local temperature is currently a hot topic. This work selects one of the nine agricultural divisions in China, the Sichuan Basin and surrounding regions, as the study area. By combining long-term series satellite remote sensing products with the space-and-time method, the spatial and temporal variations of the actual biophysical effects of LCC on land surface temperature (LST) are obtained. The results show that: (1) From 2001 to 2020, LCCs from Savannas to Cropland, from Cropland to Savannas, and from Savannas to Mixed Forest occurred frequently within the study area, and their area proportions of the total conversions are 21.7%, 18.5%, and 17.6%, respectively. (2) The biophysical feedback of LCC in the study area led to a LST increase of 0.01 ± 0.004 K at annual scale, which presents a seasonal pattern of “strong warming in summer and autumn yet weak cooling in winter”. It can exacerbate 14.3% or alleviate 8.3% of the background climate warming effect, illustrating the importance of biophysical effects on local climate change. The interaction between savannas and cropland or mixed forest and urbanizations formed the main driver for the above patterns. (3) Both the occurrence area of LCC and the warming effects at annual or seasonal scale show a trend of “first rising and then declining”, whereas the cooling effect in winter exhibits continuous enhancement over time. The monodirectional or mutual conversion between cropland and savannas is the dominant conversion responsible for these temporal patterns. The findings can provide realistic scientific guidance for informing rational policies on land management and targeted strategies for climate change response in the study area.

Keywords: land surface temperature; biophysical effects; land cover change; Sichuan Basin and surrounding regions



Citation: Mao, X.; Tang, G.; Du, J.; Tian, X. Biophysical Effects of Land Cover Changes on Land Surface Temperature on the Sichuan Basin and Surrounding Regions. *Land* **2023**, *12*, 1959. <https://doi.org/10.3390/land12111959>

Academic Editor: Charles Bourque

Received: 27 August 2023

Revised: 16 October 2023

Accepted: 19 October 2023

Published: 24 October 2023



Copyright: © 2023 by the authors. Licensee MDPI, Basel, Switzerland. This article is an open access article distributed under the terms and conditions of the Creative Commons Attribution (CC BY) license (<https://creativecommons.org/licenses/by/4.0/>).

1. Introduction

Global warming has become a tremendous challenge for human society, especially in recent years when global land surface temperature (LST) has repeatedly broken its historical records [1,2], which accompanied a large number of conversions between multiple land cover types resulting from human activities and natural disturbances [3]. In fact, there is a close interaction between these two major phenomena. On the one hand, land cover change (LCC) can influence the concentration of greenhouse gases in the atmosphere through biogeochemical processes, thereby impacting temperatures on a global scale [4]. On the other hand, LCCs affect surface radiative and non-radiative forcing by altering biophysical properties such as surface albedo and roughness, leading to LST change on a local scale [5]. However, quantifying the impacts of biophysical processes precisely is still challenging and remains a challenge in global climate change study [6].

Compared with climate model simulations and field observations, remote sensing technology can obtain real observational information over large areas at a lower cost. There-

fore, it is being increasingly utilized in the study of how the biophysical feedback from LCC impacts LST [7]. Currently, there are two main methods for quantifying the biophysical feedback of temperature. The first adopts the idea of space-for-time substitution, wherein the temperature difference between two adjacent areas with different land cover types is used as a virtual representation of the biophysical effect of LCCs [8–10]. For example, the LST difference between adjacent open land and forest represents the effects of deforestation (temperature of grassland minus temperature of forest) or afforestation (temperature of forest minus temperature of grassland), respectively [11,12]. However, this method does not involve actual type conversions and can only provide potential impacts corresponding to an ideal and complete conversion. In reality, LCCs (especially at large spatial scales) are generally gradual and incomplete, so the potential impacts obtained from the space-for-time substitution method can overestimate the strength of vegetation conversion and are usually used as reference information for possible impacts [13]. The second method employs a combination of spatial and temporal approaches (i.e., the space-and-time method), estimating the impact of LCC on temperature by comparing temperature signals where conversions occurred with those in nearby areas where no conversion occurred [4,14]. Unlike the space-for-time substitution method which only requires spatial information, this method also relies on time information about the occurrence of cover type conversion events. As a result, it can provide a more valuable policy reference by capturing the true impact on temperature. Unfortunately, existing large-scale studies often use coarse spatial resolution (e.g., 0.05°) land cover data or LST data, which makes it challenging to capture enough vegetation conversion pixels to support effective analysis, thereby limiting the widespread use of this method in practice [7]. Overall, although the space-for-time method can only provide potential “marginal impacts”, it remains the dominant approach in existing research.

The biophysical effects of LCC on LST have gained widespread attention. Research on this topic usually focuses on individual type conversions; however, the majority of research has centered around forest changes which have strong disturbance capabilities [11,15–17], though some other studies have also analyzed land surface changes by cropland expansion [10,18,19] and shrub invasion [20]. Currently, there is still a lack of comprehensive studies involving all types of conversions. Regarding the research areas, previous work focusing on China (a country with numerous hotspots of LCCs) has mainly concentrated on analyzing the Northeast region [21,22], the Northern arid and semi-arid regions [19,23], the Loess Plateau [13,24], and the Southern regions of China [16,25]. The Sichuan Basin and its surrounding regions, which are one of China’s nine major agricultural divisions and an important ecological conservation area in Southwest China, have received little attention in terms of research on the impact of LCC on LST. In this context, this study utilizes high-resolution (1-km) remote sensing data to overcome data scarcity. By employing the space-and-time approach, we aim to reveal the actual impact of all LCCs on LST in the Sichuan Basin and its surrounding regions. Taking into account the representativeness of the study area, the findings can be extrapolated to similar regions worldwide. Overall, the work is intended to provide targeted guidance for land use management, ecological environment protection, and climate change response policies.

2. Materials and Methods

2.1. Study Area

The Sichuan Basin and its surrounding regions are situated between 97° E to 110° E and 26° N to 34° N (Figure 1). The area is mainly composed of the administrative regions of Sichuan Province and Chongqing Municipality. This area borders the Qinghai–Tibet Plateau, Yunnan–Guizhou Plateau, Qinling Mountains, and Wushan Mountains, resulting in complex terrain with significant elevation variations. The landscape types include high mountains, hills, plains, and basins. The region experiences diverse climate types, encompassing subtropical monsoon climate, highland temperate climate, and tropical rainforest climate. Its annual mean temperature is between -5°C to 18°C and annual

mean precipitation is about 1037.5 mm [26]. As one of China's nine major agricultural divisions, the Sichuan Basin and its surrounding regions support a variety of agricultural production, with a focus on crops such as rice, corn, cotton, and rapeseed. However, due to the prevalence of mountainous and hilly areas, the distribution of cultivated land is fragmented with small-scale farming. This, in turn, leads to significant land use pressure and frequent land cover conversion. The consequent intense LST variation makes it one of the most ecologically vulnerable regions in Southwest China, facing severe challenges [27].

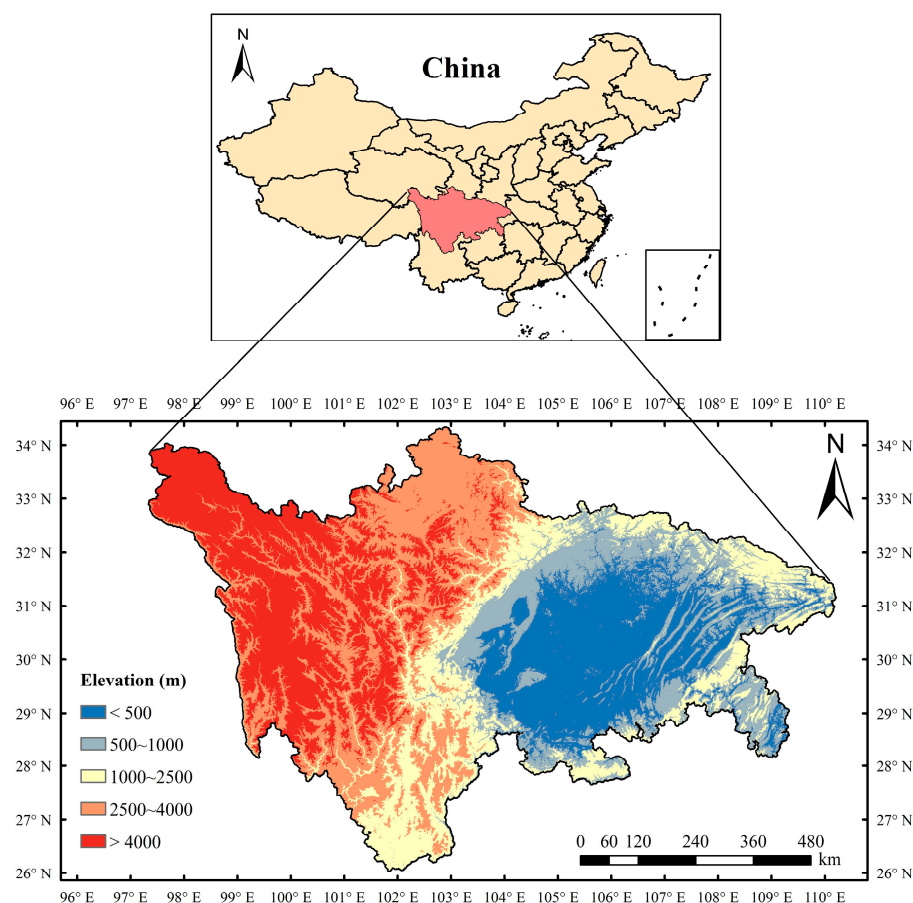


Figure 1. The location and topography of the Sichuan Basin and surrounding regions.

2.2. Data

The study utilized the MODIS (Moderate Resolution Imaging Spectroradiometer) Global Land Cover Type product, i.e., MCD12Q1, for the years between 2001 and 2020 to obtain yearly land cover information at a spatial resolution of 500 m (<https://ladsweb.modaps.eosdis.nasa.gov/search/> (accessed on 12 May 2022)). The product combines observations from both the Terra and Aqua satellites in the morning and afternoon, respectively. The MCD12Q1 data are generated using an ensemble supervised classification method of which the base algorithm is a decision tree, and ensemble classifications are estimated using boosting and further processed with various prior knowledge and ancillary information to improve classification accuracy [28]. It provides six classification systems including the International Geosphere-Biosphere Programme (IGBP) and the Food and Agriculture Organization of the United Nations (FAO). The dataset in conformity with the IGBP classification standard (ID = 1) was used. To make the results clearer, the land surface was reclassified into several major types by combining similar subtypes (summarized in Table 1). For instance, woody savanna and savanna were categorized as savannas. Ultimately, nine land cover types were identified relevant to LCC in the study area (Evergreen needleleaf

forest, Evergreen broadleaf forest, Deciduous broadleaf forest, Mixed Forest, Savannas, Grassland, Cropland, Urban, and Bare Soil).

Table 1. Table of land cover classification.

Abbreviation	Class	Subclass
ENF	Evergreen Needleleaf Forests	/
EBF	Evergreen Broadleaf Forests	/
DBF	Deciduous Broadleaf Forests	/
MF	Mixed Forests	/
SAV	Savannas	Woody Savannas Savannas
GRA	Grassland	/
CRO	Cropland	Croplands Cropland/Natural Vegetation Mosaics
URB	Urban	/
BAR	Bare Soil	/

Currently, satellite-derived LST data can only provide instantaneous temperatures under clear sky conditions when satellites transit. Although LSTs in these moments have certain indicative significance, for example, the day/night transit time of the afternoon satellite is approximately the moment of maximum/minimum temperature within a day, the temperature can still fluctuate with surrounding environmental variations, leading to significant uncertainties in the analysis [29]. Unlike previous studies that used instantaneous temperature for analysis [4,15,16,19,21], this study utilized monthly averaged LST to reflect temperature responses to LCCs. The dataset is produced based on 1-km resolution MODIS temperature products (MOD11A1 and MYD11A1), incorporating one multi-temporal weighted average transformation model and two temporal aggregation strategies (i.e., average by observation and average by daily mean temperature). The dataset also takes into account the influence of clear sky conditions. For more specific details, please refer to Liu et al. (2023) [30]. Compared to the common two-moment simple averaging method [5,31], the monthly average LST dataset produced by Liu et al. has more complete spatial coverage and higher inversion accuracy. The time span for the LST data is between 2001 and 2020, in accordance with that of the land cover dataset, and can be freely accessed (<https://zenodo.org/record/6618442#.YqB1UoRByUI> (accessed on 20 August 2022)) [32].

2.3. Methods

2.3.1. Identification of Pixels with Land Cover Change

Previous research indicated that the inter-annual variations determined by the MCD12Q1 data may not accurately reflect the actual transitions [33]. Although the Collection-6 version of the product has improved data stability by using a Markov chain model for post-processing [34], the accurate mapping of land cover has not been perfectly achieved [28]. Therefore, we implemented a two-step processing procedure to further alleviate this problem. Firstly, from a spatial consistency perspective, it is necessary to upscale the 500-m MCD12Q1 data to 1 km to match the LST data. A 1-km pixel is considered valid only if it contains at least three 500-m pixels with identical land cover type to improve the confidence level of the land cover type data [35]. Secondly, from a temporal consistency perspective, a 1-km pixel that maintains the same land cover type for several consecutive years is more reliable than those with a one-year result [14]. We set a threshold of five years to determine the initial type and converted type, meaning that only the land cover that remained unchanged for at least five years can be marked as a valid sample. Accordingly, the pixels that have undergone a LCC are identified using 10-year data (i.e., maintaining one type for the first five years and transitioning to another type for the following five years), instead of considering only the changes between two consecutive years. From

2001 to 2020, there are 11 ten-year sliding time windows (e.g., 2001–2010, 2002–2011, . . . , 2011–2020), allowing us to obtain a total of 11 pairs of LCC data.

2.3.2. Quantification of Actual LST Effect

For a central pixel which has undergone LCC, its local-scale LST variation can be considered as a combination of the impact of background climate and land type conversion [4]. With this assumption, the temperature variation of pixels that did not experience type conversion is entirely determined by the background climate. Furthermore, different pixels within an appropriate neighborhood are generally presumed to share the same background climate [7,8,11,21], and the temperature variation of adjacent pixels with the same initial land cover type as that of the central pixel, while without type conversion, are borrowed to estimate the background climate impact of the LCC. Therefore, for a central converted pixel i , the biophysical effect on temperature ($Infl_i$) can be estimated using the following formula:

$$Infl_i = \Delta T_i - \text{mean}(\Delta T_{NC,i}) \quad (1)$$

where ΔT_i represents the total LST variation of pixel i , and $\text{mean}(\Delta T_{NC,i})$ is the average LST variation of nearby pixels that have not undergone LCC. It can be seen that the $\text{mean}(\Delta T_{NC,i})$ is crucial in calculating $Infl_i$. In line with previous research [4,9], this study sets a 9 km \times 9 km sliding window as the neighborhood range. Additionally, to mitigate the influence of other factors like terrain, this study further applies inverse distance weighting to compute $\text{mean}(\Delta T_{NC,i})$. It should be noted that if there are not enough neighboring pixels with stable land cover, the target LCC pixel would be discarded.

For the entire study area, the comprehensive impact of LCC ($Infl_{all}$) is calculated using an area-weighted approach, as shown in Equation (2):

$$Infl_{all} = \frac{\sum_{t=i}^m \sum_{i=1}^n Infl_i \times Area_i}{\sum_{t=i}^m \sum_{i=1}^n Area_i} \quad (2)$$

where $Area_i$ is the area of pixel i in the study area, n is the number of pixels with the t -th type of LCC, and m is the total number of types of different LCCs.

Furthermore, it is necessary to analyze the contributions of different LCCs to the overall impact on the total study area, which is described as the relative impact of type t ($RInfl_t$), as shown in Equation (3):

$$RInfl_t = \frac{\sum_{i=1}^n Infl_i \times Area_i}{\sum_{t=i}^m \sum_{i=1}^n Area_i} \quad (3)$$

where the symbols have the same meanings as in Equation (2). By comparing Equations (2) and (3), it can be observed that the sum of the relative impacts of different LCCs is equal to the comprehensive impact on the entire study area. In other words, the combined effects of various LCCs on LST in the study area can be determined by adding up their respective relative impacts.

Moreover, it is necessary to select an appropriate temperature change indicator. Previous studies have used various methods to represent temperature change information, such as the difference between the average temperatures of two consecutive periods [25], the difference between the temperature of the first year of the first period and the last year of the second period [4], or the trend of temperature change over the study period [14]. In order to obtain relatively stable temperature change results, the difference between the average LST of the last 5 years and the average LST of the previous 5 years is calculated as the indicator to characterize temperature changes.

3. Results

3.1. Overview of Land Cover Change

From 2001 to 2020, a total of 16,633 1-km pixels in the Sichuan Basin and surrounding regions underwent LCCs, accounting for approximately 2.9% of the total study area. Among them, 12,486 pixels (75.1%) experienced one type of conversion, 4004 pixels (24.1%) experienced two types of conversion, and less than 1% of the pixels underwent three or four types of conversion. In total, there are 22 different types of conversions.

Combining Figure 2a with Figure 1, it can be observed that the two most prominent conversion types are the interactions between Savannas and Cropland (cropland expansion and cropland reduction account for 21.7% and 18.5% of total conversions, respectively). These conversions are mainly concentrated in the Sichuan Basin (at elevations below 500 m), followed by the conversion from Savannas to Mixed Forest, accounting for 17.6% of total conversions, and distributed in the undulating mountains on the eastern, southern, and northern sides of the Sichuan Basin (at elevations between 500 and 1000 m). The conversion from Grassland to Savannas also accounts for over 10% of total conversions, while these pixels exhibit no clustering pattern and are scattered in the high undulating mountains in the western region (at elevations above 2500 m). The conversion from Mixed Forest to Savannas and from Savannas to Deciduous Forest account for around 5% of total conversions, which are distributed in the western and northern regions of the Sichuan Basin in low undulating mountains (at elevations between 1000 and 2500 m). The remaining 16 types of conversions are predominantly scattered in high undulating mountains at elevations above 4000 m and together account for 20.9% of total conversions. Furthermore, according to Figure 2b, only the interaction between Savannas and Cropland exhibits a relatively higher conversion degree, meaning that within a 5-km pixel, there are more than five 1-km pixels that have undergone land cover changes.

3.2. The Spatial Distribution of the Impact of Land Cover Change on LST

Figure 3 shows the LST variations for pixels with cover type conversion within the study area. In terms of overall impact between 2001 and 2020, the biophysical feedback of LCC causes a local LST increase of 0.01 ± 0.004 K at the annual scale (Figure 3a). It also exhibits distinct seasonal patterns, with LST changes of 0.01 ± 0.000 K in spring, 0.02 ± 0.004 K in summer, 0.02 ± 0.002 K in autumn, and -0.01 ± 0.006 K in winter, indicating that LCC leads to a local LST response characteristic of “warmer in summer and colder in winter”. Furthermore, compared to the space-for-time method, the space-and-time method has the advantage of capturing the background climate impact at the same location and time period, allowing for a more intuitive reflection of the magnitude and sign of the biophysical effects of LCC [4,13]. As shown in Figure 3b, unlike the LST response from cover changes, the background climate exerts a local warming effect both at the annual scale (0.18 ± 0.024 K) and in the four seasons (0.30 ± 0.022 K, 0.18 ± 0.019 K, 0.14 ± 0.025 K, and 0.12 ± 0.026 K in spring, summer, autumn, winter, respectively), while it shows a decreasing trend in the magnitude of its impact from spring to winter. Comparing the biophysical feedback of type conversion to that of the background climate influence, the ratio of them is only 5.6% (0.01 K/ 0.18 K) at the annual scale, indicating a relatively insignificant effect. However, when examining different seasons, the ratios increase to 11.1% in summer and 14.3% in autumn, and particularly in winter, where the biophysical feedback mitigates the background climate’s warming effect by 8.3%. This highlights the significant role of LCC in mitigating or exacerbating the impacts of climate change.

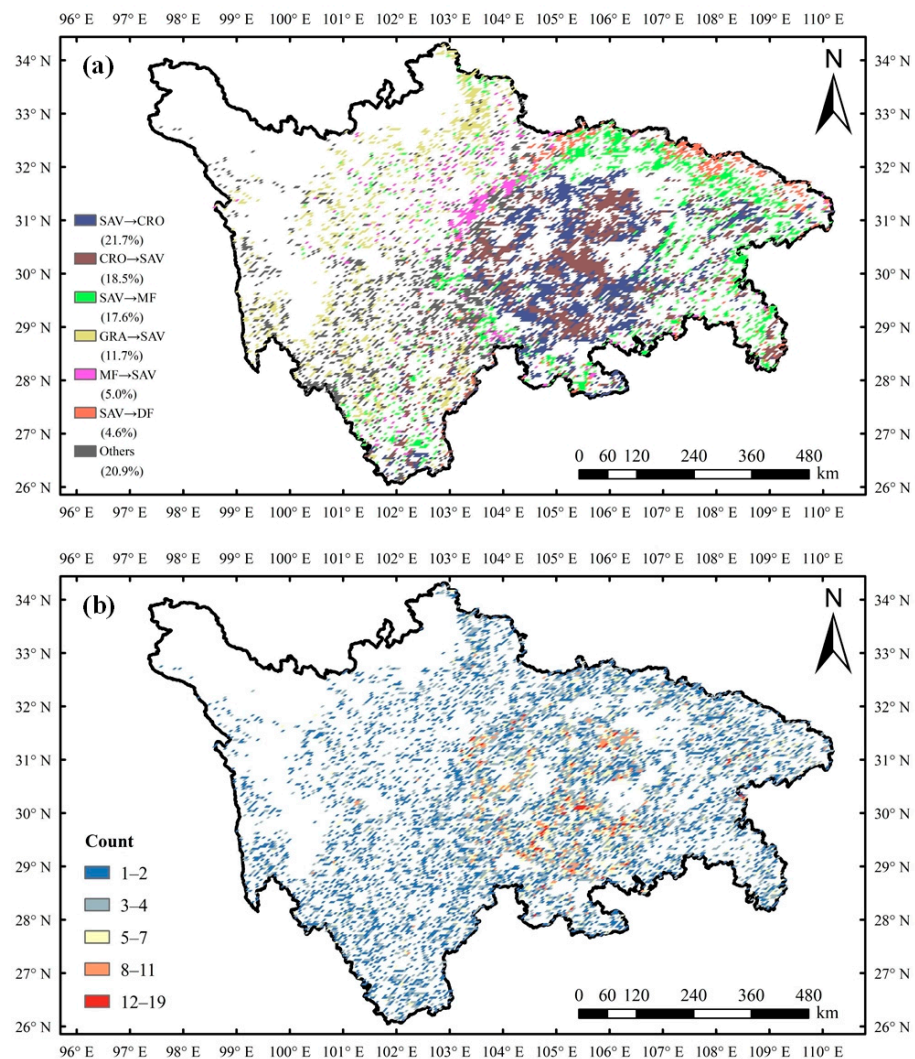


Figure 2. Overall land cover change in the Sichuan Basin and surrounding regions. For display purposes, the original 1-km pixels were upscaled to 5 km. (a) The spatial distribution of the main conversion types, i.e., the conversion with the largest area within a 5-km pixel, where the percentages in the legend represent the proportion of the conversion type area to all conversion pixels. (b) The count of 1-km pixels that have undergone cover type conversion within a 5-km pixel. SAV, CRO, MF, GRA, and DF are abbreviations for Savannas, Cropland, Mixed Forest, Grassland, and Deciduous Forest, respectively.

Based on the grid map in Figure 3a, it is evident that the mutual conversion between cropland and sparse grassland has the largest relative impact, where the annual effect of cropland reduction is 0.012 ± 0.002 K, while the annual effect of cropland expansion is -0.009 ± 0.002 K. Compared to Savannas, the cooling effect brought by cropland is mainly attributed to increased irrigation or evapotranspiration [36,37]. According to Figure 2a, the conversion area from Savannas to Cropland (21.7%) is larger than that from Cropland to Savannas (18.5%), indicating that the cooling effect per unit area due to cropland expansion is smaller than the warming effect caused by cropland reduction. This further emphasizes the importance of preserving cropland. Moreover, the significant summer warming effect (0.021 ± 0.001 K) caused by the conversion from Cropland to Savannas and the strong winter cooling effect (-0.011 ± 0.003 K) caused by the conversion from Savannas to Cropland are the primary cause for the seasonal disparity in LST effects across the entire study area.

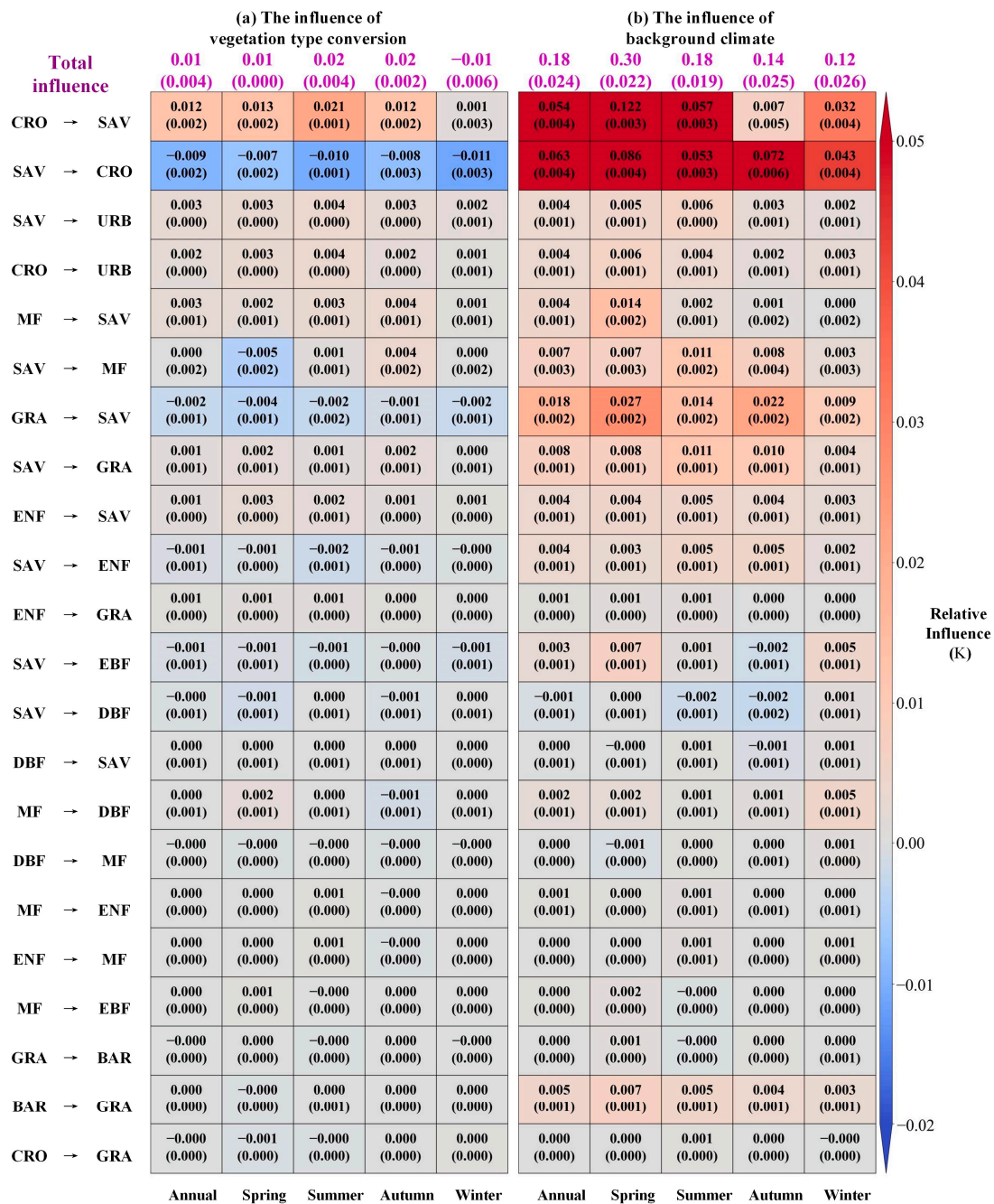


Figure 3. The changes in land surface temperature for pixels with land cover changes in the Sichuan Basin and surrounding regions from 2001 to 2020. (a) The biophysical influences of land cover change, and (b) the influences of background climate change. The numbers in magenta represent the overall effect for the entire study area, whereas the grids show the relative effect of each conversion type. The numbers in parentheses represent standard errors. SAV, CRO, URB, MF, GRA, DBF, ENF, EBF, and BAR are abbreviations for Savannas, Cropland, Urban, Mixed Forest, Grassland, Deciduous Broadleaf Forest, Evergreen Needleleaf Forest, Evergreen Broadleaf Forest, and Bare Soil, respectively.

Urbanization also has a significant LST impact, with the conversion from Savannas to Urban land causing a relative warming effect of 0.003 ± 0.000 K at annual scale, and the conversion from Cropland to Urban land causing a relative warming effect of 0.002 ± 0.000 K at annual scale. The areas of these two conversions are relatively small (Figure 2a), accounting for only 0.79% and 0.64% of the total converted pixels; however, the fact that such minor proportions can lead to significant relative impacts highlights the powerful

warming effect of urbanization. Although urbanization leads to a local LST increase at the annual averaged level, it exhibits stronger warming in summer than in winter, which also facilitates the overall summer warming in the entire study area. The findings are consistent with previous studies on the seasonality of urban heat island effects [38,39], demonstrating the reliability of the analysis in this study.

The mutual conversion between Mixed Forests and Savannas also shows noticeable relative impacts, especially in autumn, where both conversions result in a warming effect of 0.004 K. This is the main reason for the seasonality of their impact in the study area. The absence of the opposing effects in these two reverse conversions may be attributed to their different locations. According to Figure 2a, the conversion from Savannas to Mixed Forests is distributed in the eastern, southern, and northern mountainous regions of the Sichuan Basin (at altitudes between 500 and 1000 m), while the conversion from Mixed Forests to Savannas is distributed in the western mountainous regions of the Sichuan Basin (at altitudes between 1000 and 2500 m). In addition, Savannas are complex grassland ecosystems typically composed of continuous grasses with scattered trees or shrubs, and Mixed Forest is a type of forest ecosystem where different species of trees coexist and intermingle [40]. The complicated components of Savannas and Mixed Forest may also result in similar LST impact in their mutual conversions. Moreover, the mutual conversion between Savannas and Grassland/Evergreen Needleleaf Forests, the conversion from Evergreen Needleleaf Forests to Grassland, and the conversion from Savannas to Evergreen Broadleaf Forests also contribute significantly to the overall LST effect in the study area (with absolute values of annual relative impact ranging from 0.001 K to 0.002 K). On the other hand, the mutual conversion between Savannas and Deciduous Broadleaf Forests, the internal forest conversions (i.e., Mixed Forests interconverted with Deciduous Broadleaf Forests, Evergreen Needleleaf Forests, and Deciduous Broadleaf Forests), the mutual conversion between Grassland and Bare Soil, and the Grassland reversion from Cropland produce a weak contribution to the overall impact in the study area (with relative impacts close to 0 K).

3.3. The Temporal Pattern of the Impact of Land Cover Change on LST

According to Figure 4a, the area of LCC in the Sichuan Basin and its surrounding regions shows an obvious trend of “first rising and then declining” from 2001 to 2020, and the peak occurred in the sliding time window from 2004 to 2013, with a conversion area of 2492 km². The annual impact on LST also exhibits a similar trend of “first rising and then declining”, while the peak occurs in the two windows of 2005–2014 (0.03 ± 0.008 K) and 2006–2015 (0.03 ± 0.007 K). On the seasonal scale, the LST impact in spring, summer, and autumn also follows the “first rising and then declining” trend. The peak value occurred in the window of 2005–2014 for spring (0.03 ± 0.005 K), and the window of 2006–2015 for summer (0.05 ± 0.006 K) and autumn (0.04 ± 0.005 K), resulting in the abovementioned two peaks on the annual scale. In contrast, the LST impact in winter is mostly a cooling effect and exhibits a significant monotonic decreasing trend with a slope of -0.002 K ($p < 0.05$). This phenomenon indicates that the winter cooling effect caused by LCC in the study area is continuously strengthening over time.

To explore the reasons for the temporal variations in area and temperature impact, the trends of area and relative impact of each type of conversion over time were further analyzed. According to Figure 5, the conversion area from Cropland to Savannas shows a similar “rising first and then declining” pattern in area variation to that for the overall area (with a high correlation coefficient of 0.92), which is the determinant for the overall area variation in the study area (Figure 4a). As for the temperature impact, as shown in Figure 6e, the conversion from Savannas to Cropland basically determines the continuous enhancement of the winter cooling effect (with a correlation coefficient of 0.70). However, on the other hand, for the other three seasons and the annual scale (Figure 6a–d), the conversion from Savannas to Cropland is not the predominant influence on determining the overall performance. Instead, the combined effects of mutual conversions between

Cropland and Savannas show a similar temporal variation pattern to the overall impact (with correlation coefficients of 0.74, 0.76, 0.72, and 0.69 for the annual, spring, summer, and autumn scales, respectively).

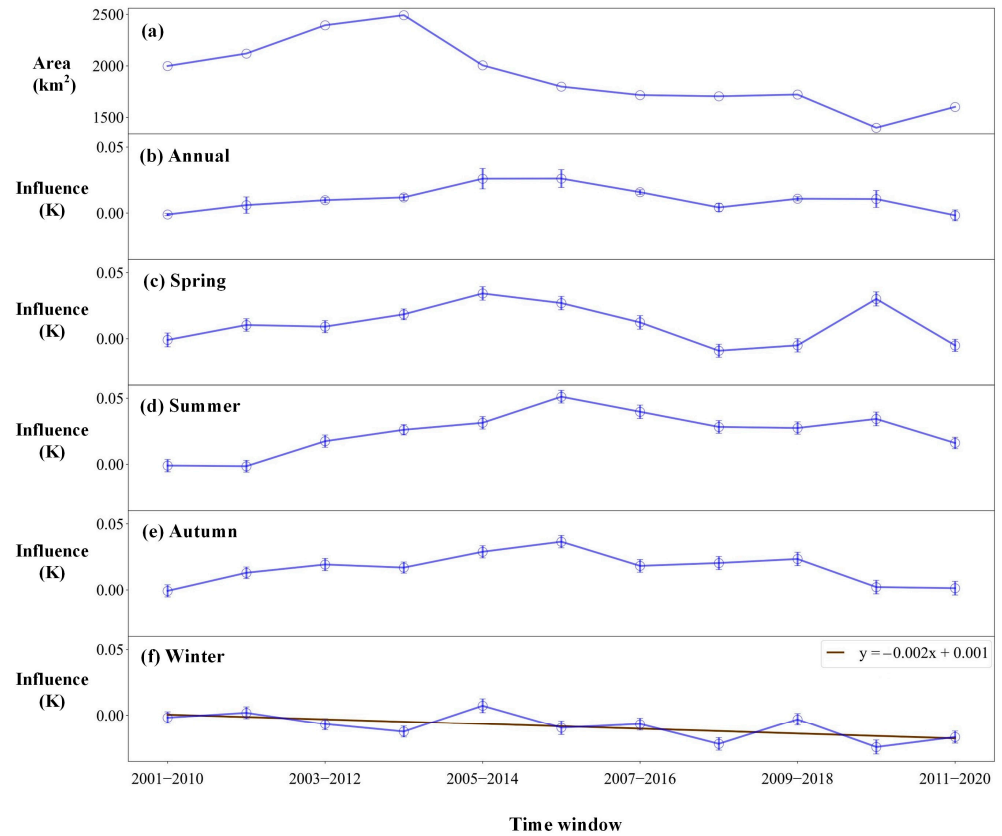


Figure 4. The temporal variations of occurrence area and biophysical temperature effects in the Sichuan Basin and surrounding regions. (a) Area changes over time, (b–f) temperature changes over time for the annual, spring, summer, autumn, and winter seasons, respectively. The error bars represent standard errors of the corresponding influences, and the slope was calculated at the significant interval of 95% ($p < 0.05$).

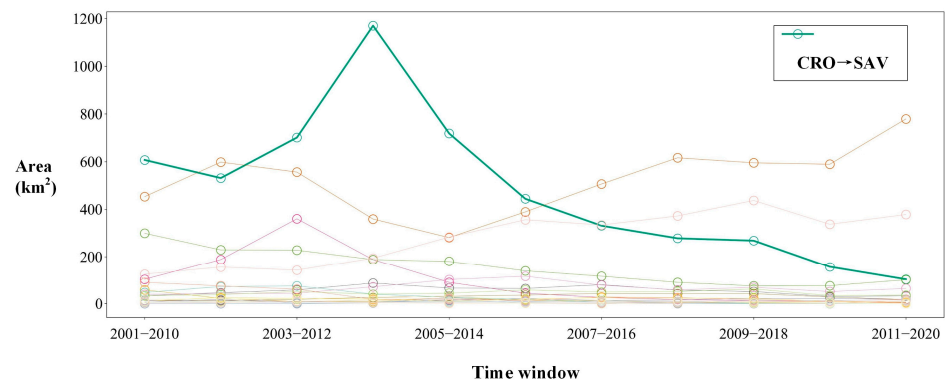


Figure 5. The temporal variations of occurrence area for each land cover change in the Sichuan Basin and surrounding regions. Different colors represent different conversions, and the bold line with green color is the conversion from Cropland (CRO) to Savannas (SAV).

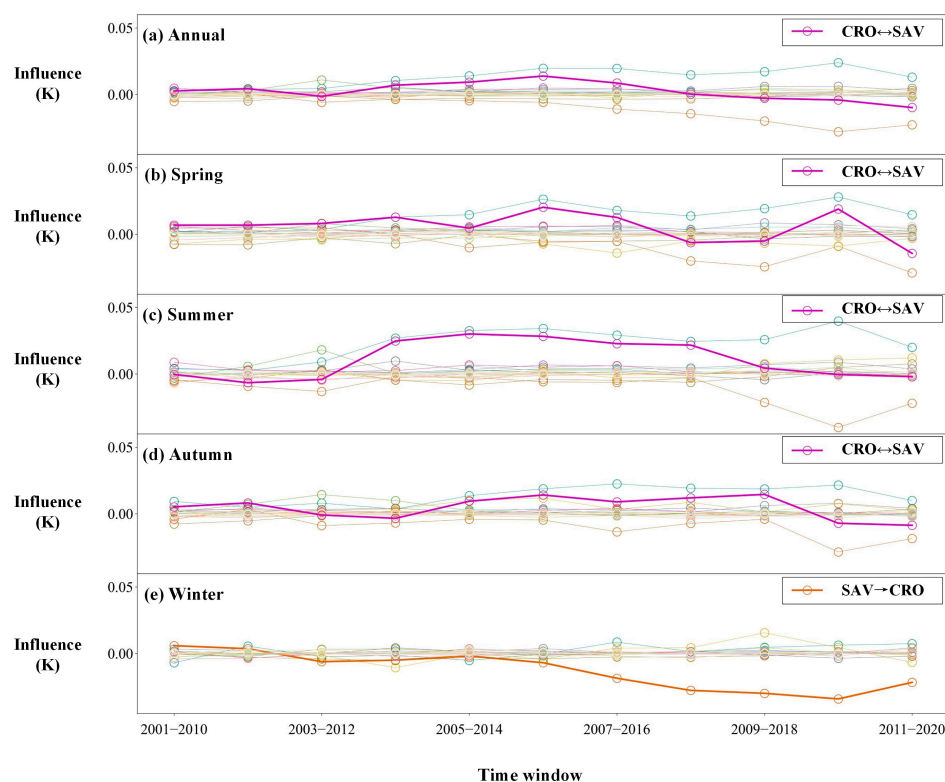


Figure 6. The temporal variations of biophysical temperature effect for each land cover change in the Sichuan Basin and surrounding regions. (a–e) are the results for the annual, spring, summer, autumn, and winter averages, respectively. Different colors represent different conversions, the bold lines with purple color in (a–d) are the mutual changes between Cropland (CRO) and Savannas (SAV), and the bold line with orange color in (e) is the conversion from SAV to CRO.

4. Discussion

This study primarily centered on assessing the influence of LCCs on LST within the Sichuan Basin and its neighboring areas. Nevertheless, these findings can be substantiated by prior research on both a global and regional scale related to LST. For regional LST change in some areas with similar geographic and climatic conditions to those in the Sichuan basin, the cropland areas are coldest relative to impervious surfaces [41]. It was parallel with our finds regarding LCCs, which reminds us of the negative effect of urban sprawl into agricultural land and should be taken into account in policy making. Specifically, the warming effect of urban areas showed similar seasonal LST variation patterns as that in the urban heat island effect [38,42,43]. In terms of the LST impact on human well-being, the methods and findings are also indicative for global climate mitigation and food security. As temperature variation was proved to impact agricultural yields, more cautions should be paid to regions with distinct LCCs and LST change [44].

The study provides realistic insights into the actual impacts, rather than the potential envelope effects [13], of LCCs on LST. However, the magnitude of overall LST changes on the annual scale remains relatively small (i.e., 0.01 K). There are three possible reasons for this phenomenon. Firstly, it is important to note that the land cover data used in this study are not flawless. The classification system employed in the MCD12Q1 data may introduce some inaccuracies into analyses relying on this product, especially when evaluating LCC in forested regions [45], which constitute the primary land cover types in our study area. Secondly, according to the analysis in Sections 3.1–3.3, conversions involving Savannas played a dominant role in both the spatial and temporal variations of LST impact. As mentioned in Section 3.2, Savannas are a complex grassland ecosystem containing multiple cover components. Hence, the conversions from Savannas to other

types may involve complex internal conversions of different covers; for example, the conversion from Savannas to Cropland may be the conversion from internal Grassland to Cropland, while the conversion from Savannas to Broadleaf Forest may come from the reduction in a large number of internal trees. According to Figure 3, these conversion types showed very weak relative impacts, resulting in an overall insignificant effect. Last but not least, the study area is characterized by mountainous and hilly terrain with small and fragmented parcels, leading to a relatively low degree of land cover conversion. Previous research has shown an approximate linear relationship between the conversion degree and its LST impact [13], meaning that a lower conversion degree can ultimately lead to a smaller LST impact. To overcome these limitations, employing higher-resolution land cover data, such as the 30-m resolution Globe30 product [46], to calculate the LST impact of land cover conversion at the pure pixel level rather than the mixed pixel level as in this study may be a more feasible approach.

5. Conclusions

Based on satellite remote sensing land cover and monthly averaged LST data from 2001 to 2020, this study focused on the impact of LCCs on LST in one of China's nine major agricultural divisions, the Sichuan Basin and surrounding regions. The main conclusions are as follows:

- (1) From 2001 to 2020, approximately 2.9% of the pixels in the study area underwent LCCs, and the distribution of different conversion types was mainly regulated by altitude. The most prevalent conversion was the interaction between Savannas and Cropland within the Sichuan Basin.
- (2) During 2001–2020, the biophysical feedback of LCCs led to an annual average LST increase of 0.01 ± 0.004 K, which exhibited a seasonal pattern of strong warming in summer and autumn and weaker cooling in winter. Overall, these conversions can exacerbate or alleviate the background climate warming effect of about 10%. The main reasons to the above patterns were the conversions between Savannas and Cropland, between Mixed Forest and Savanna, and in urbanization.
- (3) Both the area of LCCs and the warming impact on annual and seasonal scales demonstrated a “first rising and then declining” trend over time. However, the cooling impact in winter showed a continuous enhancement trend. The monodirectional or mutual conversions between Cropland and Savannas were the dominant factors driving the temporal pattern of variations in area and temperature impact.

Author Contributions: Conceptualization, X.M. and G.T.; methodology, X.M.; formal analysis, J.D.; investigation, X.T.; data curation, X.M.; writing—original draft preparation, X.M.; writing—review and editing, G.T.; supervision, G.T. All authors have read and agreed to the published version of the manuscript.

Funding: This research received no external funding.

Data Availability Statement: The land cover and monthly mean land surface temperature data supporting the reported results can be found and downloaded at <https://ladsweb.modaps.eosdis.nasa.gov/search/> (accessed on 12 May 2022) and <https://zenodo.org/record/6618442#.YqB1UoRByUI> (accessed on 20 August 2022), respectively.

Acknowledgments: The authors are grateful to NASA for providing the land cover data.

Conflicts of Interest: The authors declare no conflict of interests.

References

1. Thompson, A. NASA Says 2020 Tied for Hottest Year on Record. 2021. Available online: <https://www.scientificamerican.com/article/2020-will-rival-2016-for-hottest-year-on-record/> (accessed on 4 September 2023).
2. Susskind, J.; Schmidt, G.A.; Lee, J.N.; Iredell, L. Recent global warming as confirmed by AIRS. *Environ. Res. Lett.* **2019**, *14*, 044030. [CrossRef]

3. Winkler, K.; Fuchs, R.; Rounsevell, M.; Herold, M. Global land use changes are four times greater than previously estimated. *Nat. Commun.* **2021**, *12*, 2501. [[CrossRef](#)] [[PubMed](#)]
4. Alkama, R.; Cescatti, A. Biophysical climate impacts of recent changes in global forest cover. *Science* **2016**, *351*, 600–604. [[CrossRef](#)] [[PubMed](#)]
5. Li, Y.; Li, Z.-L.; Wu, H.; Zhou, C.; Liu, X.; Leng, P.; Yang, P.; Wu, W.; Tang, R.; Shang, G.-F.; et al. Biophysical impacts of earth greening can substantially mitigate regional land surface temperature warming. *Nat. Commun.* **2023**, *14*, 121. [[CrossRef](#)] [[PubMed](#)]
6. Perugini, L.; Caporaso, L.; Marconi, S.; Cescatti, A.; Quesada, B.; de Noblet-Ducoudre, N.; House, J.I.; Arneth, A. Biophysical effects on temperature and precipitation due to land cover change. *Environ. Res. Lett.* **2017**, *12*, 053002. [[CrossRef](#)]
7. Duveiller, G.; Hooker, J.; Cescatti, A. The mark of vegetation change on Earth's surface energy balance. *Nat. Commun.* **2018**, *9*, 679. [[CrossRef](#)] [[PubMed](#)]
8. Lee, X.; Goulden, M.L.; Hollinger, D.Y.; Barr, A.; Black, T.A.; Bohrer, G.; Bracho, R.; Drake, B.; Goldstein, A.; Gu, L.; et al. Observed increase in local cooling effect of deforestation at higher latitudes. *Nature* **2011**, *479*, 384–387. [[CrossRef](#)] [[PubMed](#)]
9. Li, Y.; Zhao, M.; Motesharrei, S.; Mu, Q.; Kalnay, E.; Li, S. Local cooling and warming effects of forests based on satellite observations. *Nat. Commun.* **2015**, *6*, 6603. [[CrossRef](#)]
10. Zhou, D.; Xiao, J.; Frohling, S.; Liu, S.; Zhang, L.; Cui, Y.; Zhou, G. Croplands intensify regional and global warming according to satellite observations. *Remote Sens. Environ.* **2021**, *264*, 112585. [[CrossRef](#)]
11. Wang, L.; Duan, S.-B.; Zhang, X.; Chang, S.; Liu, X.; Huang, C.; Qian, Y.G. The influence of afforestation on land surface temperature in China. *Natl. Remote Sens. Bull.* **2021**, *25*, 1862–1872. [[CrossRef](#)]
12. Liao, W.; Rigden, A.J.; Li, D. Attribution of local temperature response to deforestation. *J. Geophys. Res. Biogeosci.* **2018**, *123*, 1572–1587. [[CrossRef](#)]
13. Wang, H.; Yue, C.; Luysaert, S. Reconciling different approaches to quantifying land surface temperature impacts of afforestation using satellite observations. *Biogeosciences* **2023**, *20*, 75–92. [[CrossRef](#)]
14. Li, Y.; Zhao, M.; Mildrexler, D.J.; Motesharrei, S.; Mu, Q.; Kalnay, E.; Zhao, F.; Li, S.; Wang, K. Potential and Actual impacts of deforestation and afforestation on land surface temperature. *J. Geophys. Res. Atmos.* **2016**, *121*, 14372–14386. [[CrossRef](#)]
15. Ge, J. Biogeophysical Impacts of Large-Scale Ecological Programs on Regional Climate in China. Ph.D. Thesis, Nanjing University, Nanjing, China, 2019.
16. Shen, W.; He, J.; Huang, C.; Li, M. Quantifying the Actual Impacts of Forest Cover Change on Surface Temperature in Guangdong, China. *Remote Sens.* **2020**, *12*, 2354. [[CrossRef](#)]
17. Zeng, Z.; Wang, D.; Yang, L.; Wu, J.; Ziegler, A.D.; Liu, M.; Ciais, P.; Searchinger, T.D.; Yang, Z.-L.; Chen, D.; et al. Deforestation-induced warming over tropical mountain regions regulated by elevation. *Nat. Geosci.* **2021**, *14*, 23–29. [[CrossRef](#)]
18. Shen, X.; Liu, B.; Jiang, M.; Lu, X. Marshland loss warms local land surface temperature in China. *Geophys. Res. Lett.* **2020**, *47*, e2020GL087648. [[CrossRef](#)]
19. Liu, W.; Dong, J.; Du, G.; Zhang, G.; Hao, Z.; You, N.; Zhao, G.; Flynn, K.C.; Yang, T.; Zhou, Y. Biophysical effects of paddy rice expansion on land surface temperature in Northeastern Asia. *Agric. For. Meteorol.* **2022**, *315*, 108820. [[CrossRef](#)]
20. Shen, X.; Liu, Y.; Liu, B.; Zhang, J.; Wang, L.; Lu, X.; Jiang, M. Effect of shrub encroachment on land surface temperature in semi-arid areas of temperate regions of the Northern Hemisphere. *Agric. For. Meteorol.* **2022**, *320*, 108943. [[CrossRef](#)]
21. Di, W.; Shen, R.; Huang, A.; Han, H. Analysis of the Biophysical Mechanism of Cooling/Warming Effect of Cropland Expansion on Land Surface Temperature in Northeast China. *China J. Agrometeorol.* **2022**, *43*, 450–463.
22. Liu, X.; Tong, X.; Shi, X.; Yang, J.; Gu, J. Impact of farming on land surface temperature over Northeast China. *J. PLA Univ. Sci. Technol.* **2015**, *16*, 97–102.
23. Zhu, H.; Zhang, Y.; Shen, X.; Wang, S.; Shang, L.; Su, Y. A numerical simulation of the impact of vegetation evolution on the regional climate in the ecotone of agriculture and animal husbandry over China. *Plateau Meteorol.* **2018**, *37*, 721–733.
24. Tian, L.; Zhang, B.; Wang, X.; Chen, S.; Pan, B. Large-Scale Afforestation Over the Loess Plateau in China Contributes to the Local Warming Trend. *J. Geophys. Res. Atmos.* **2021**, *127*, e2021jd035730. [[CrossRef](#)]
25. Shen, W.; Li, M.; Huang, C.; He, T.; Tao, X.; Wei, A. Local land surface temperature change induced by afforestation based on satellite observations in Guangdong plantation forests in China. *Agric. For. Meteorol.* **2019**, 276–277, 107641. [[CrossRef](#)]
26. Shao, J.; Li, Y.; Ni, J. The characteristics of temperature variability with terrain, latitude and longitude in Sichuan-Chongqing Region. *J. Geogr. Sci.* **2012**, *22*, 223–244. [[CrossRef](#)]
27. Liu, Y.; Zhang, Z.; Wang, J. Regional differentiation and comprehensive regionalization scheme of modern agriculture in China. *Acta Geogr. Sin.* **2018**, *73*, 203–218.
28. Sulla-Menashe, D.; Gray, J.M.; Abercrombie, S.P.; Friedl, M.A. Hierarchical mapping of annual global land cover 2001 to present: The MODIS Collection 6 Land Cover product. *Remote Sens. Environ.* **2019**, *222*, 183–194. [[CrossRef](#)]
29. Li, Z.L.; Wu, H.; Duan, S.B.; Zhao, W.; Ren, H.; Liu, X.; Leng, P.; Tang, R.; Ye, X.; Zhu, J. Satellite remote sensing of global land surface temperature: Definition, methods, products, and applications. *Rev. Geophys.* **2023**, *61*, e2022RG000777. [[CrossRef](#)]
30. Liu, X.; Li, Z.L.; Li, J.H.; Leng, P.; Liu, M.; Gao, M. Temporal upscaling of MODIS 1-km instantaneous land surface temperature to monthly mean value: Method evaluation and product generation. *IEEE Trans. Geosci. Remote Sens.* **2023**, *61*, 5001214. [[CrossRef](#)]
31. Xing, Z.; Li, Z.-L.; Duan, S.-B.; Liu, X.; Zheng, X.; Leng, P.; Gao, M.; Zhang, X.; Shang, G. Estimation of daily mean land surface temperature at global scale using pairs of daytime and nighttime MODIS instantaneous observations. *ISPRS J. Photogramm. Remote Sens.* **2021**, *178*, 51–67. [[CrossRef](#)]

32. Liu, X.; Li, Z.; Li, J.; Leng, P.; Liu, M.; Gao, M. *Global 1-km Monthly Mean Land Surface Temperature Product (2003–2020)*; Zenodo: Geneva, Switzerland, 2022; (1.0). [[CrossRef](#)]
33. Friedl, M.A.; Sulla-Menashe, D.; Tan, B.; Schneider, A.; Ramankutty, N.; Sibley, A.; Huang, X. MODIS Collection 5 global land cover: Algorithm refinements and characterization of new datasets. *Remote Sens. Environ.* **2010**, *114*, 168–182. [[CrossRef](#)]
34. Abera, T.A.; Heiskanen, J.; Pellikka, P.; Rautiainen, M.; Maeda, E.E. Clarifying the role of radiative mechanisms in the spatio-temporal changes of land surface temperature across the Horn of Africa. *Remote Sens. Environ.* **2019**, *221*, 210–224. [[CrossRef](#)]
35. Liu, X.; Tang, B.-H.; Li, Z.-L. Evaluation of three parametric models for estimating directional thermal radiation from simulation, airborne, and satellite data. *Remote Sens.* **2018**, *10*, 420. [[CrossRef](#)]
36. Tang, T.; Lee, X.; Schultz, N.; Zhang, K.; Cai, L.; Lawrence, D.M.; Shevliakova, E. Biophysical Impact of Land Use and Land Cover Change on Subgrid Temperature in CMIP6 Models. *J. Hydrometeorol.* **2022**, *24*, 373–388. [[CrossRef](#)]
37. Yang, Q.; Huang, X.; Tang, Q. Global assessment of the impact of irrigation on land surface temperature. *Sci. Bull.* **2020**, *65*, 1440–1443. [[CrossRef](#)] [[PubMed](#)]
38. Si, M.; Li, Z.-L.; Nerry, F.; Tang, B.-H.; Leng, P.; Wu, H.; Zhang, X.; Shang, G. Spatiotemporal pattern and long-term trend of global surface urban heat islands characterized by dynamic urban-extent method and MODIS data. *ISPRS J. Photogramm. Remote Sens.* **2022**, *183*, 321–335. [[CrossRef](#)]
39. Lu, Y.; Yang, J.; Huang, X.; Yang, Q.; Ma, S. Effects of Urban Morphology on Land Surface Temperature in Local Climate Zones. *Geomat. Inf. Sci. Wuhan Univ.* **2021**, *46*, 1412–1422. [[CrossRef](#)]
40. Loveland, T.R.; Belward, A. The international geosphere biosphere programme data and information system global land cover data set (DISCover). *Acta Astronaut.* **1997**, *41*, 681–689. [[CrossRef](#)]
41. Shahfahad; Bindajam, A.A.; Naikoo, M.W.; Horo, J.P.; Mallick, J.; Rihan, M.; Malcoti, M.D.; Talukdar, S.; Rahman, R.; Rahman, A. Response of soil moisture and vegetation conditions in seasonal variation of land surface temperature and surface urban heat island intensity in sub-tropical semi-arid cities. *Theor. Appl. Climatol.* **2023**, *153*, 367–395. [[CrossRef](#)]
42. Dong, R.; Wurm, M.; Taubenböck, H. Seasonal and diurnal variation of land surface temperature distribution and its relation to land use/land cover patterns. *Int. J. Environ. Res. Public Health* **2022**, *19*, 12738. [[CrossRef](#)]
43. Shi, Z.; Yang, J.; Wang, L.-e.; Lv, F.; Wang, G.; Xiao, X.; Xia, J. Exploring seasonal diurnal surface temperature variation in cities based on ECOSTRESS data: A local climate zone perspective. *Front. Public Health* **2022**, *10*, 1001344. [[CrossRef](#)]
44. Kafy, A.-A.; Rahman, A.F.; Al Rakib, A.; Akter, K.S.; Raikwar, V.; Jahir, D.M.A.; Ferdousi, J.; Kona, M.A. Assessment and prediction of seasonal land surface temperature change using multi-temporal Landsat images and their impacts on agricultural yields in Rajshahi, Bangladesh. *Environ. Chall.* **2021**, *4*, 100147.
45. Zhao, J.; Dong, Y.; Zhang, M.; Huang, L. Comparison of identifying land cover tempo-spatial changes using GlobCover and MCD12Q1 global land cover products. *Arab. J. Geosci.* **2020**, *13*, 792. [[CrossRef](#)]
46. Jun, C.; Ban, Y.; Li, S. Open access to Earth land-cover map. *Nature* **2014**, *514*, 434. [[CrossRef](#)]

Disclaimer/Publisher’s Note: The statements, opinions and data contained in all publications are solely those of the individual author(s) and contributor(s) and not of MDPI and/or the editor(s). MDPI and/or the editor(s) disclaim responsibility for any injury to people or property resulting from any ideas, methods, instructions or products referred to in the content.